Deep Spatial Interpolation of Rain Field for U.K. Satellite Networks

Guangguang Yang, Zebin Chen, David L. Ndzi, Linda Yang, Abdul-Hadi Al-Hassani, David C. Paul, Zhikui Duan, and Jun Chen

Abstract—This article presents two new state-of-the-art spatial rain field interpolation convolutional neural networks (SRFICNNs), referred to as learned deviation (LD) and learned interpolation (LI) models, for predicting the point rain rate at finer spatial scales. The main contribution is the successful introduction of the prior-art deep learning technique into high-resolution (HR) rainfall rate prediction with significant improvement in accuracy. This is very important for the effective implementation of fade mitigation techniques for both terrestrial and satellite networks. The comparison of the models' performances with ground truth (radar measurements) shows that the proposed models give an excellent mean square error (MSE) and structural SIMilarity (SSIM) in rainfall field reconstruction if the network depth falls in the range of 15–25 weight layers. The final model uses 20 layers for HR point rain rate prediction. Further study shows that the LD model offers a faster convergence and yields a more accurate rain rate prediction. In particular, this article compares the rain rate exceedance distribution and Log-Normality property from the model estimates with values calculated from measured data. Results show that the LD model gives a highly accurate estimate of these two indices with the corresponding root mean square (rms) error of 5.1709×10^{-4} and 0.0013, respectively.

Guangguang Yang is with the School of Electronic Information Engineering, Foshan University, Foshan 528225, China, also with the School of Computing, University of Portsmouth, PO1 3HE Portsmouth, U.K., and also with Guangdong Daoli AI Technology Ltd., Guangzhou 510700, China (e-mail: sunshineuop@qq.com).

Zebin Chen is with the School of Computer Science and Engineering, Sun Yat-sen University, Guangzhou 510006, China (e-mail: zebinchen018@foxmail.com).

David L. Ndzi is with the School of Computing Engineering and Physical Sciences, University of West of Scotland, PA1 2BE Paisley, U.K. (e-mail: david.ndzi@uws.ac.uk).

Linda Yang is with the School of Computing, University of Portsmouth, PO1 3HE Portsmouth, U.K. (e-mail: linda.yang@port.ac.uk).

Abdul-Hadi Al-Hassani is with the Chancellor's Office, Iraq University College, Basrah, Iraq (e-mail: hadi.alhassani@iuc.edu.iq).

David C. Paul is with the Chartered Institute of Marketing, M15 5RL Manchester, U.K. (e-mail: david.paul@imarco.com).

Zhikui Duan is with the School of Electronic Information Engineering, Foshan University, Foshan 528000, China (e-mail: duanzhikui@outlook.com).

Jun Chen is with the School of Computer Science, Sun Yat-sen University, Guangzhou, Guangdong 510006, China, and also with the School of Industrial Design and Ceramic Art, Foshan University, Foshan 528000, China (e-mail: chenj269@mail2.sysu.edu.cn).

Color versions of one or more figures in this article are available at https://doi.org/10.1109/TAP.2022.3229175.

Digital Object Identifier 10.1109/TAP.2022.3229175

Index Terms—Depth, radio-wave propagation, rainfall rate, receptive field, satellite communication, spatial rain field interpolation convolutional neural networks (SRFICNNs).

I. INTRODUCTION

RAIN absorbs and scatters microwave signals at frequencies above 10 GHz leading to signal attenuation and reduction of terrestrial and satellite communication systems availability [1], [2].

The planning and design of next-generation satellite network systems require high space-resolution rain data to accurately predict the attenuation statistics. This is particularly true for the effective implementation of some applications, i.e., fade mitigation techniques (FMTs), site diversity techniques, and the prediction of instantaneous joint fade experienced by all the links in an arbitrary microwave network [3], [4]. However, high-space-resolution rain data are often unavailable for wide areas, and the cost of such measurements is prohibitive [5]. This fundamental issue has stymied progress in rain modeling for a long time. To address this problem, many interpolation algorithms have been proposed over the last few decades. For example, the Random Midpoint Displacement algorithm (RMD) developed by Voss [6] is one of the widely used interpolation techniques. It improves the space resolution by introducing new rain rate samples at new locations without changing the underlying distribution. The fractal theory [7] has also attracted a significant amount of attention and has been applied to the study of rain since the mid-1980s [8]. Many studies have demonstrated that rain inherits fractal properties over a range of scales, and this is strongly favored for rain modeling [9], [10], [11]. For example, the multi-fractal model developed by Xu et al. [12] can interpolate the Tropical Rainfall Measurement Mission (TRMM) rain products to finer space scales with reasonable accuracy. The averaging theory-based downscaling model is an alternative technique that has attracted significant attention from researchers. For example, Luini and Capsoni [13] investigated the effect of space and/or time integration on the spatial correlation functions of rain. Also, the authors' previous work proposed a new interpolation approach with a comprehensive study of four key rain characteristics using the averaging theory as well [14]. It provides a wide range of space and/or time resolution rain field simulations for Northwest Europe with high levels of accuracy.

Despite progress in rain study over the last few decades, there are severe limits to what can be accurately simulated.

This mainly stems from the extremely high variability of rainfall, causing difficulty in explicitly grasping the underlying properties of rain distribution. Therefore, artificial neural networks (ANNs) have been used to assist in rain modeling. For example, Sharifi et al use three downscaling algorithms, including ANNs, to predict the high space resolution rain rate in Northeast Australia [11]. Also, based on ANNs, a model proposed by Ayo et al. [15] can forecast real-time rain attenuation and serve as a good tool for satellite-based digital transmission systems in South Africa. In recent advances, deep learning, particularly the convolutional neural networks (CNNs), is proving to be a major breakthrough and a highly powerful tool to automatically discover the features needed for detection or classification with a very little engineering. Deep learning has been extensively applied in multidisciplinary fields, including image processing [16], object detection [17], and precipitation forecasting [18]. Results show that CNNs are highly effective in extracting feature representations from raw data by interleaving convolutional and pooling layers. In the wake of this success in many other fields and thanks to the increased data availability and computational resources, the use of deep learning is now finally being applied to rain study as well. Knowing that rain is highly variable in both space and time leading to non-linear or chaotic spatio-temporal variations, it is logical to claim that no single interpolation or downscaling method can be considered efficient enough for fine-scale rain rate prediction. In data with complex topographies, quasi-periodicities, and non-linearities, such as rain, deep learning-based methods provide a potential solution in interpolating apparatus-derived observation into higher resolutions. This is because such a method is capable of exploiting the underlying distribution of rain learned exclusively from historical radar measurements, instead of handcrafting the rain characteristics that are designed based mainly on mathematical models, such as those in [12], [19], and [20]. Therefore, deep learning is highly suitable for the study of rain. However, only a few studies that have applied the CNNs technique to rain modeling have been reported in the open literature. A representative model developed by Polz et al. [21] has proved that CNNs are a robust and promising tool in detecting both rain events and rain-induced attenuation patterns in commercial microwave links covering all of Germany on an hourly basis. Another example is the study presented in [22] for which the authors employed three deep learning-based algorithms to produce $4\times$ times higher resolution rainfall data during the summer monsoon season. It shows that deep learning-based methods provide an efficient solution in downscaling rainfall data to high spatial resolution.

The lack of high-resolution (HR) rain rate data has long been a challenging issue for accurate performance prediction of satellite and terrestrial high-frequency network links over wide areas. This is primarily due to the high variability of rain which impacts the accuracy of rain attenuation modeling. From open literature, there are very limited studies of rain that employ the strength of deep learning, although these new techniques can potentially be more accurate than traditional ones. Inspiringly, the recent developments, i.e., [23], [24], in the super-resolution (SR) of a single image have pointed out

a new direction in interpolating rain estimates into high space resolution. In this article, we have proposed two new deep learning-based models. These are the learned interpolation (LI) model and the learned deviation (LD) model, with the help of the CNNs technique. The key objective is to develop a new method for predicting rain rate at finer spatial scales and provide a new approach to studying rain-induced attenuation for radio-wave propagation and wireless communication.

The rest of this article is organized as follows. Section II describes the data used in this study, and Section III presents the methodology proposed. We also describe the data pre-processing in detail and introduce the general architecture of the proposed spatial rain field interpolation CNNs (SRFICNNs) technique. The experimental results achieved from the proposed models are presented in Section IV. Here, we analyze the model prediction from a computer vision perspective and provide simulated rainfall fields for visualization. Section V validates the models' performance from three aspects; error percentage, rain rate exceedance, and log-Normality property, to show the accuracy of the proposed models. The advantages and disadvantages of deep learning-based rain modeling are further discussed in Section VI. Conclusions are drawn in Section VII.

II. Data Description

The experimental data used in this study is provided by the Centre for Environmental Data Analysis (CEDA). One of its databases is provided by the U.K. Meteorological Office NIMROD radar system which has 15 C-band rainfall weather radar installations covering the whole of the British Isles. NIMROD data is continuously updated and CEDA ensures the long-term integrity of the data. Four to five radars repeat the scan at different elevations to build 3-D scans of the area from which the best estimates of rain rates on the ground are established (details about the NIMROD radar system are given in [25]). The U.K. rainfall rate estimates are recorded on a grid matrix of 1725×2175 km. The rain field maps are continuously generated at a sampling interval of 5 min while the coverage of each grid point varies from 1×1 km to 5×5 km depending on the distance to the nearest radar. In addition, the NIMROD data has been validated using rain gauge measurements, and a range of data is used to calibrate the radars. Although there are some differences between radar estimates and rain gauge data due to spatial averaging, this does not affect the accuracy significantly. For example, the 1 km NIMROD data has been shown to yield unbiased estimates of annual 0.01% exceed rain rates [26].

Fig. 1 shows a typical composite rain rate image of the U.K. The gray color is the area outside the range of the radar network where no rain data is available, and the black color represents the scanned area where data can be obtained. Each image ranges from 46.7343° to 60.4010° in latitude and $-14.0766°$ to 8.4178° in longitude.

The NIMROD system uses data collected from range/height indicator (RHI) scans at several elevations to estimate the rain rates at different altitudes and combines these datasets to predict the rain rate at ground level. However, the ground rain rates are not quantized because complex spatial-temporal
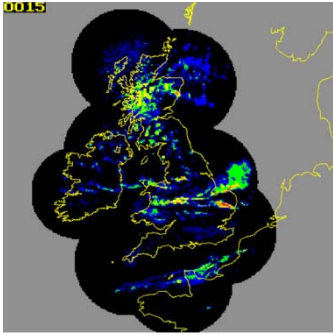
Fig. 1. NIMROD composite images of precipitation rates for the British Isles with 1 km sampling.

processing is always involved, see [27]. Given that applications in radio propagation require knowledge of rain variation over much shorter spatial scales, i.e., a typical Fresnel zone of a few tens of meters, the majority of meteorological data cannot meet this requirement. So a new approach that can address this problem is required to predict rain rates at finer scales. In this study, we computed 8436 (one month) continuous 5 km NIMROD radar data to develop deep learning-based models for predicting the up-scaled rain fields. We contrasted and validated the models' performance by comparing the results with the measurements achieved from 1 km U.K. rain rate data.

III. METHODOLOGY

A. Rainfall Rate

Accurate prediction of rain attenuation statistics requires a good understanding of rain, particularly those at finer scales. According to Rec. ITU-R P. 838-3 [28], the relationship between specific attenuation γ (dB/km) and rainfall rate R (mm/h) along the links can be approximately defined as a power-law model

$$\gamma \cong \alpha R^\beta \tag{1}$$

where α and β are the parameters related to frequency, wave polarization, and link elevation angle.

The accuracy and resolution of attenuation γ (dB/km) strongly depend on the rainfall rate, R, since α and β are only frequency-related [29]. Knowing that the rainfall rate at a given location $\mathbf{x} = [x_1, x_2]$ refers to the amount of rain that falls over an interval of time assuming that the rainfall intensity over that time period was constant. The NIMROD composite rain maps are represented on a Cartesian grid and each point contains the area-time averaged rain intensity. Therefore, the instantaneous averaged rainfall rate centered on a grid point with an area of $A = L^2$ over time T can be expressed as in [30]

$$R(L, T) = \frac{1}{AT} \int_{-\frac{T}{2}}^{\frac{T}{2}} dt \int_{-\frac{L}{2}}^{\frac{L}{2}} \int_{-\frac{L}{2}}^{\frac{L}{2}} r(\mathbf{x}, t) da \tag{2}$$

where $r(\mathbf{x}, t)$ represents the point rainfall rate at location $\mathbf{x}$ and time t on a 2-D Cartesian grid. The intervals T and L are the temporal and spatial integration lengths, respectively.

If interval T is fixed, then (2) can be simplified to describe the instantaneous area-averaged rainfall rate at time t, that is,

$$R(t) = \frac{1}{A} \int_{-\frac{L}{2}}^{\frac{L}{2}} \int_{-\frac{L}{2}}^{\frac{L}{2}} r(\mathbf{x}, t) da. \tag{3}$$

The key objective of the designed SRFICNNs is to obtain the rate estimates at L' ($L' < L$).

B. Pre-Processing of NIMROD Radar Data

The raw NIMROD radar data must be pre-processed before training and testing the designed CNNs. The main processing includes partitioning, cropping, and augmentation, see details as follows.

1) Partitioning: As aforementioned in the literature, deep learning generally benefits from big data training. Following the proportion division that is widely used in the CNNs design, i.e., [23], we split the NIMROD data into three independent subsets. The first is the training dataset, which is used to fit the model parameters, so-called weights. This subset includes 7592 radar images, so the network has sufficient data to learn. CNN requires the input and output to be of the same size and hence this part of the data is up-scaled to the desired size—the one held by 1 km data, using some technique (i.e., bicubic interpolation [24]). The second is the validation dataset. It provides an unbiased evaluation of a model fit to the training dataset while tuning the model's hyperparameters (i.e., the number of hidden units—layer depths and channel widths). This subset is used for regularization by stopping early and the optimization of model parameters. It efficiently prevents the model from overfitting the training data. The rest of the data is the testing dataset (reference label), which is used as ground truth for assessing the final model selected during the validation process. In particular, it should be highlighted that the division follows the random sampling principle and no repeated sampling is allowed. The random sampling principle ensures the fairness of the experiment and avoids the occasionality caused by human intervention, while the non-repeatability guarantees that the three sub-datasets are mutual-exclusive and independent so no adverse effect on the outcome will happen.

2) Cropping: The original radar maps span irregular-shaped areas covered by the radars, and contain large gray areas where data is unavailable, see Fig. 2(a). Such areas do not contribute to network training and are excluded from training. Note that the radar estimates are mainly available for the continental areas, so data beyond the radar scan range, typically the oceanic areas, are not involved in the model development. In addition, using the data from regularly shaped areas can significantly reduce network complexity. Therefore, we cropped the original radar maps Fig. 2(a) to be Fig. 2(b), making the observed rain events to be concentrated on the majority continental part of the British Isles. This allows the extraction and modeling of the rain characteristics of each region in a better way. The size of the cropped area is 1460 × 740 km, ranging from 48.8780° to 49.0147° in latitude and −4.5507° to −3.2615° in longitude. It should
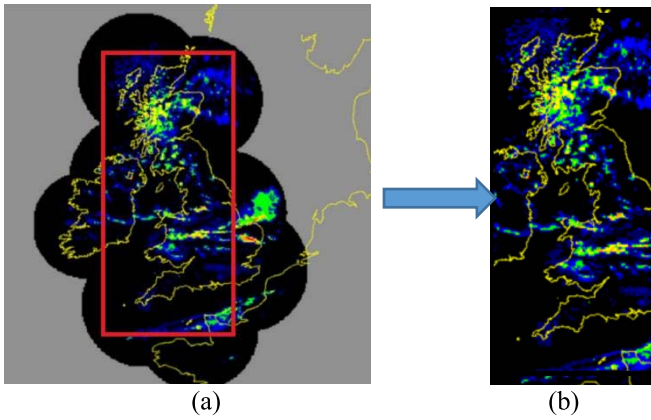
Fig. 2.   Rain field plotting of NIMROD products. (a) Original radar-derived rain map. (b) Cropped map focus on British continent.
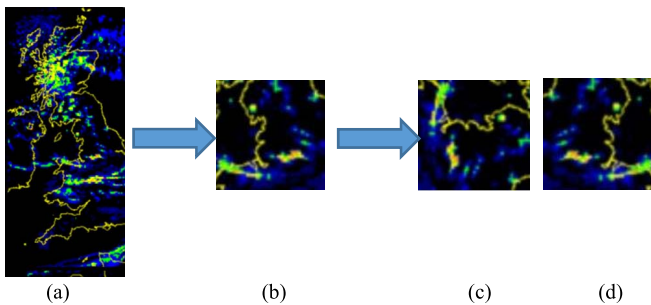

Fig. 3.   Example of data augmentation. (a) Cropped image and (b) image patch randomly extracted from (a) with grid size of 41 × 41. (c) Rotation transformation for which (b) is rotated 90° clockwise. (d) Mirror-symmetric image for (b).

be highlighted that locations with no data will be assigned 0 by default to guarantee the following processing works normally.

3) Augmentation: Using a common strategy in image processing, see [31], augmentation needs to be applied to expand the amount of data in the training set. To be specific, eight overlapping patches from the input radar map are randomly extracted and pre-processed before training. Note that the grid is 41 × 41 with the size of each patch representing an area of 205 × 205 km because the statistical distribution of rain will become stable and converge to constant values when the map size is greater than 200 × 200 km, see [32]. In particular, the sample amount is expanded via rotation transformation and horizontal flip, so the diversity of input data can be largely enhanced. Fig. 3 presents an example of data augmentation. Here, Fig. 3(b) shows one of the eight randomly extracted patches from Fig. 3(a), and each patch undergo the processing steps in Fig. 3(c) and (d) to achieve the data augmentation. This is helpful for the improvement of the models' robustness.

C. Convolutional Neural Network

1) Training Setup: CNN, as a feed-forward neural network, is trained by a supervised learning method [33]. Batches of samples are passed through the network and the outputs are compared to the reference labels. In this article, the batch size used is 64. After each batch, a loss function is computed and the parameters are updated according to a learning rule. From the experiment, it was found that indicators used for model assessment will converge to a stable value of around 80 epochs. Hence, in this study, the default epoch amount is set as 100, and each epoch will experience 949 iterations. Also, the scale factor (SF), the number of times that the resolution is expected to be improved, was set as 5 for validation purposes since 1 km data is available. Other SF values have also been studied although the results are not presented in this article. In particular, the Adam optimizer has been introduced to reduce the computation time. Following the study in [34], the initial learning rate was set as 0.001 and is halved every 10 epochs.

Extensive studies have demonstrated that a large receptive field can adequately capture the local correlation between the central pixel and surroundings in a wider range [35]. This is because the information contained in a small patch is insufficient for detail recovery if a large SF is applied in the model. In practice, this center-surround relation is widely used in SR image processing (i.e., [23]) since the surrounding region provides more constraints to the SR issue. With regard to the rain study, if the rain events are entirely contained in a receptive field, it is possible for the network to adequately recognize the underlying properties of rain (i.e., horizontal structure of rain field) and recover the details (rain rate at finer spatial scales) of interest. Therefore the fundamental task of CNNs is to improve the receptive field based on cascading a sequence of 3 × 3 convolution filters which operate on 3 × 3 spatial regions across 64 channels. For the depth D network, the size of the receptive field is $(2D + 1) \times (2D + 1)$ and proportional to the depth. In this study, the final D has been found to be 20 layers, so the size of the receptive field is 205 × 205 km, enabling the statistical distribution of rain to be properly captured.

2) Network Structure: The networks contain $D + 2$ layers including the input layer and the output layer, see Fig. 4. The first layer serves to receive the input data [up-scaled low-resolution (ULR) radar data with the desired size] and extracts patches for the subsequent layers. The last layer is used for the HR rain field reconstruction. D successive layers hidden in-between have two main functions; first to extract features, including the horizontal structure of rain fields, rain pattern, and distribution, from the raw model input. Early convolution layers identify simple patterns in the data, which are used to identify more complex patterns in subsequent layers. Second, very deep CNNs layers are used to determine the non-linear mapping between the low-resolution (LR) radar data and HR ones based on the rain features extracted in advance. These two functions serve the output layer to obtain the final reconstructed rainfall fields.

Rectified linear units (ReLUs) are always set as the activation function and are usually placed behind each convolution layer in CNNs for the improvement of the non-linear modeling capability of the network [36]. Following this strategy, the networks proposed in this study also adopt ReLU as the activation function to assist high-space resolution rainfall field reconstruction.
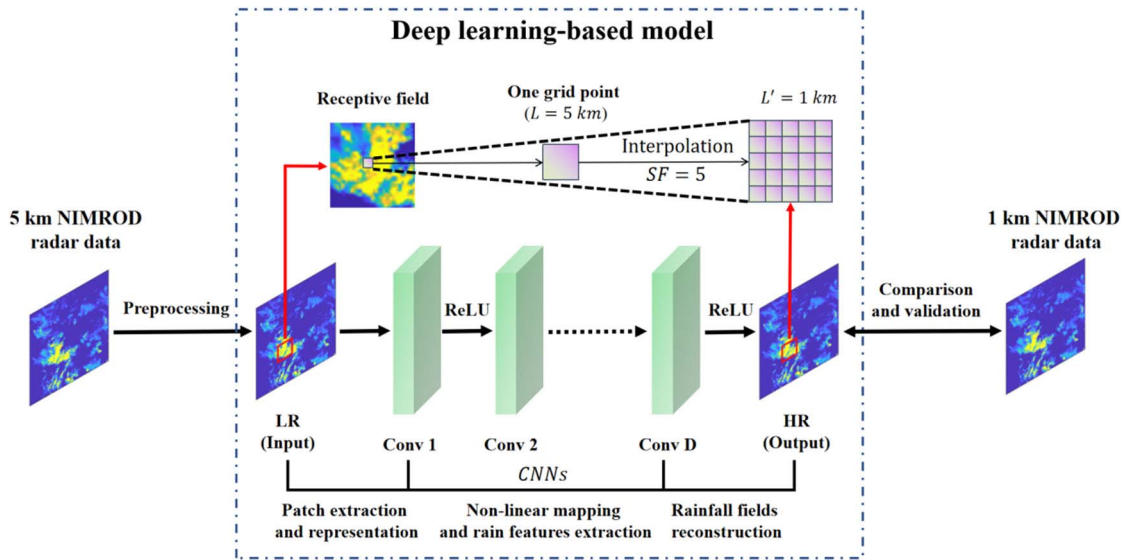
Fig. 4. Overview of the proposed approach. The left part is the raw data provided by NIMROD radar. The middle part (dashed box) is the deep learning-based rain model. As the soul of the whole model design, it uses the CNNs to grasp the underlying rain properties and the non-linear mapping relationship between LR rain map and the high one, so the HR point rainfall rate can be accurately estimated. Note that the extent that resolution is improved is dependent on the value of SF. For example, here we set the SF = 5 so the space resolution will be improved 5× times. The right part is the 1 km NIMROD data used for model comparison and validation.

3) Model Design: This section examines the two proposed deep learning-based rain models.

a) Learned interpolation model: Different from the traditional interpolation algorithms for which monotonous changing tendency is normally required to guarantee performance, the LI model is a data-driven approach that automatically learns the underlying distribution of rainfall rate and then provides reasonable predictions at new locations. To achieve this, we use CNNs to extract the changing properties of local rain intensity, and then determine the interpolated parameters to describe the local correlation amongst rain rates to improve the spatial resolution of rainfall fields. The designed network is outlined in Fig. 5(a). Dong et al. [23] have demonstrated that CNN can be used to learn to map from LR to HR in an end-to-end manner. It does not require any artificial features that are typically demanded in other methods to show its superior performance. In this study, this mapping can be described as

$$R_H \cong \mathcal{F}(R_L^*) \qquad (4)$$

where $\mathcal{F}(\cdot)$ is an indescribable non-linear mapping relation between the HR rain map (R_H) and ULR one (R_L^*). Therefore, the main task of the LI model is the determination of the $\mathcal{F}(\cdot)$ function and parameter adjustments via end-to-end learning of historical NIMROD radar records.

b) Learned deviation model: Following [24], we designed the LD model, which focuses on learning the difference (referred to as residual) between the expected HR rainfall rates and low ones, to achieve a higher learning rate [configuration is outlined in Fig. 5(b)]. This is because LR precipitation and HR one share the same information and are highly correlated to a large extent, explicitly modeling the residual is extremely advantageous. In addition, the center-surround relation also has its drawback, that is, it fails to be
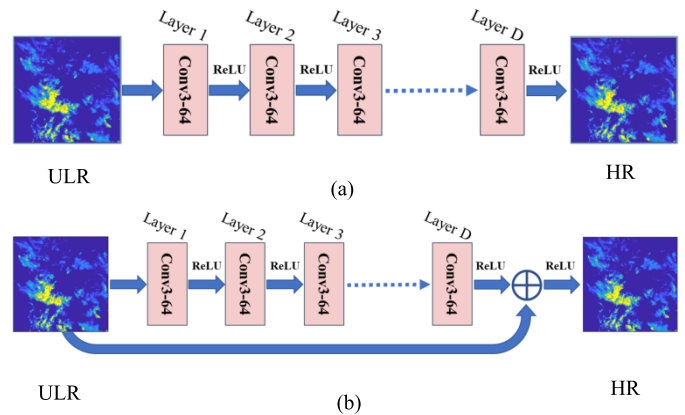

Fig. 5. Network structure. (a) LI model. (b) LD model. A series of layers (convolutional and non-linear) have been cascaded repeatedly in the network. The input (ULR NIMROD radar data) goes through layer-by-layer and transforms into a high-resolution point rainfall rate. The 64 filters for each convolutional layers and sample feature maps have been presented for visualization.

exploited to the full extent for points near the grid matrix boundary, so models will be invalid if the required surrounding region is too large. To address this problem, zero padding is used before any convolutions to keep all feature maps (channels) the same size. The details are added back to the input ULR radar data to produce the final HR rain rate once they are predicted. In general, the key point of this design is to reduce the absolute error between the LR and HR rain estimates based on the modeling of residuals. The general procedure can be mathematically described as

$$\mathcal{F}^*(R_L^*) \equiv R_H - R_L^* \qquad (5)$$
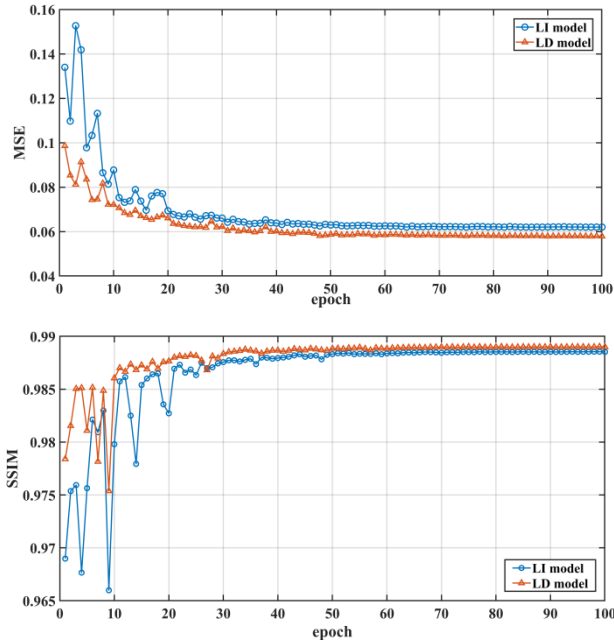
where $\mathcal{F}^*(R_L)$ is the residual.

Fig. 6. Plotting of the MSE and SSIM with changing epochs for the LI model and LD model.

IV. EXPERIMENTAL RESULTS

A. Convergence Analysis

In this study, we use two indicators; the mean square error (MSE) and the structural SIMilarity (SSIM) [38] to quantitatively evaluate the proposed models. In theory, the mathematical expression of SSIM for two images x and y is given as follows:

$$\text{SSIM}(x, y) = \frac{(2\mu_x\mu_y + c_1) + (2\sigma_{xy} + c_2)}{(\mu_x^2 + \mu_y^2 + c_1)(\sigma_x^2 + \sigma_y^2 + c_2)}. \quad (6)$$

Here, $\{\mu_x, \mu_y\}$ and $\{\sigma_x^2, \sigma_y^2\}$ are the mean and variance of x and y, respectively, and σ_{xy} stands for the covariance between x and y. c_1 and c_2 are constants used for maintaining stability.

The MSE is used to measure the difference between model predictions and NIMROD estimates with better resolution. In addition, we use the square of the difference as a loss function (L_{MSE}), that is,

$$L_{MSE} = \|R_H - R_M\|^2 \quad (7)$$

where R_H and R_M are the predicted high-resolution rain rate from the proposed models and NIMROD radar measurement, respectively.

The SSIM is widely used in image processing to measure the SSIM between two images [38]. In theory, the maximum value of SSIM is 1, so the larger the SSIM, the better the reconstruction quality. For this study, a large SSIM value means that the rainfall fields, particularly for rain events that happened at the boundary of rain fields, can be smoothly reconstructed.

Fig. 6 presents the plot of the calculated MSE and SSIM against epochs. It can be noted that the variation of the indicators of the LD model is generally smaller than those

TABLE I
CALCULATED MSE AND SSIM VALUES FOR THE PROPOSED MODELS

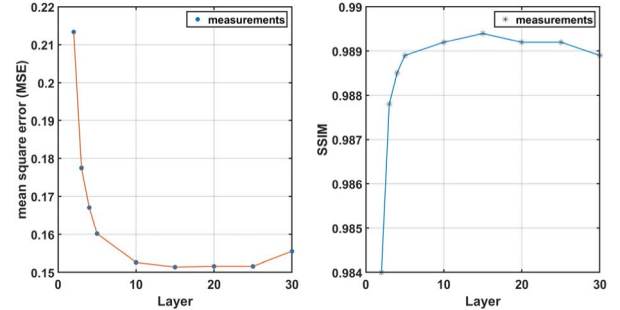| Methods	MSE	SSIM
LI model	0.1619	0.9887
LD model	0.1516	0.9892

Fig. 7. Calculated MSE and SSIM of the LD model at different layers.

of the LI model throughout the whole range of epochs. The MSE of the LD model starts to converge and becomes stable after 10 epochs while it is from 20 epochs for the LI model. The same is true for the SSIM, indicating a faster convergence speed for the LD model. This is because the LD model is based on the residual data for which most values are likely to be 0 or very small. The sparse results distribution significantly reduces the computation time. The final MSE and SSIM values are given in Table I. In general, smaller MSE and larger SSIM shows that the LD model gives superior performance.

In theory, the deeper the network, the larger the receptive fields. Therefore, it is possible to obtain knowledge of how the receptive field size affects the reconstruction quality by studying the changing network depths (D). Given that a large perimeter zone helps to boost network performance and robustness to predict rainfall rate at the central point of the receptive field, the spatial resolution of the rainfall field can be improved if rain intensity in the local area has been taken into account. Fig. 7 presents the general tendency of MSE and SSIM with increasing network layers (depth D). Both MSE and SSIM improve with an increasing number of layers until their reach optimum values in the 15–25 range. It is worth noting that both indicators get worse for numbers of layers greater than 25. It is important to balance the network depth and cost since the larger the number of layers the greater the computational power required. As a compromise, the default depth was set to 20 layers. One reason is that the calculated size of the receptive field for $D = 20$ is 41 × 41 (205 × 205 km). This enables the statistics of rain to stabilize so the models' performance can be further enhanced.

B. Rain Field Simulation

Fig. 8 presents a visual comparison of rainfall fields yielded by the proposed models and the one produced by NIMROD radar. Since the details on a large scale [see Fig. 8(a)] are very difficult to see, a zoomed-in image of a size of 100 × 100 km with heavy rain events is shown in Fig. 8(b). The rainfall fields produced by the LD model [Fig. 8(d)] are very similar to
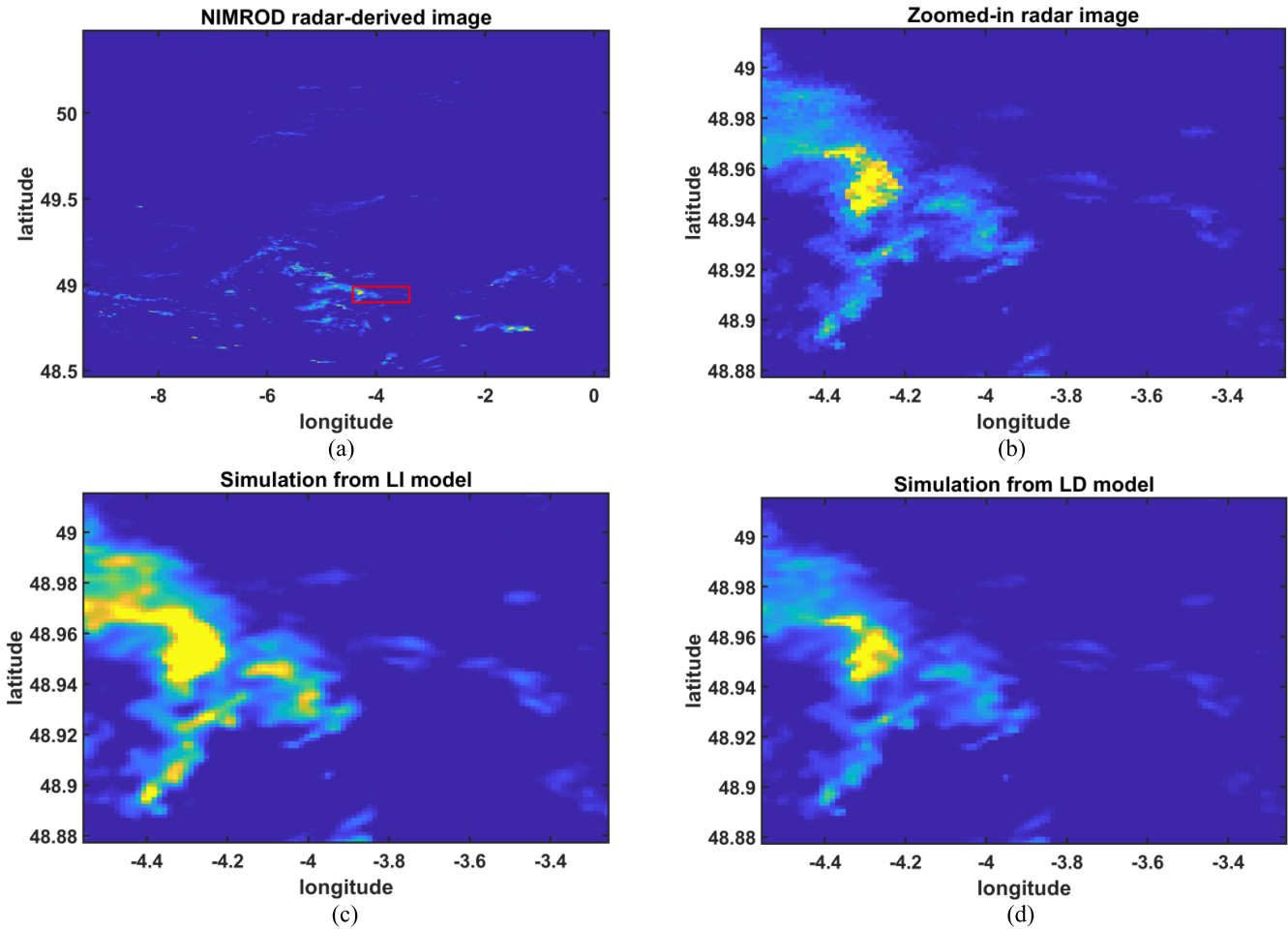
Fig. 8. Sample results of simulated rainfall fields. (a) Real NIMROD radar-derived image, (b) zoomed-in view of radar image, (c) simulated rainfall fields from LI model, and (d) simulated rainfall fields from LD model. Here, the model depth is 20 layers ($D = 20$).

the radar-derived image [Fig. 8(b)] in both rain intensity and horizontal rain field structure. However, a small difference can be observed in the high rain intensity area, see the middle left of Fig. 8(b) and (d). On the contrary, the rain rate estimates provided by the LI model show significant differences from the real measurements although the horizontal rain field structure is similar. The color area (yellow and orange) in Fig. 8(c) is much larger than the one in Fig. 8(b), indicating that the LI model tends to overestimate the point rain rate. This finding is in accordance with the rain rate exceedance distribution, see Section V.

V. VALIDATION

Comparing a model's predictions with the measured data is commonly performed to validate the model's performance. In this study, the model assessments are conducted using the error function, rain rate exceedance, and the underlying rain distribution.

A. Error Function

The error function can be defined as [38]

$$Error = \left| ln\left(\frac{R_{measured}}{R_{predicted}}\right) \right| \quad (8)$$

where $R_{measured}$ and $R_{predicted}$ are measured and the model predicted rainfall rate, respectively.

The mean $\overline{Error}$ is calculated by

$$\overline{Error} = \frac{1}{n}\sum_{i=1}^{n} Error_i \quad (9)$$

where $Error_i$ is the error for individual location and n is the number of locations. The calculated $\overline{Error}$ for the LI model is 0.0852, which is roughly 2.7 times that of the LD model for which the $\overline{Error}$ is 0.0317.

B. Rain Rate Exceedance

According to ITU Rec. P.837-7, the rain rate exceedance distribution required for propagation studies must correspond to an average year, and the percentage of exceeded rain rate between $R_{0.001}$ and $R_{0.01}$ is of particular importance [39]. Rain rates exceedance distribution can be obtained by

$$P_r\{R > r|r > 0\} = \frac{N_r}{N_T} \times 100\% \quad (10)$$

where P_r is the percentage of rain rate exceedance, N_r is the occurrence of any specific rainfall rate r ($r > 0$), and N_T is the total samples (including rain and no rain) over the studied
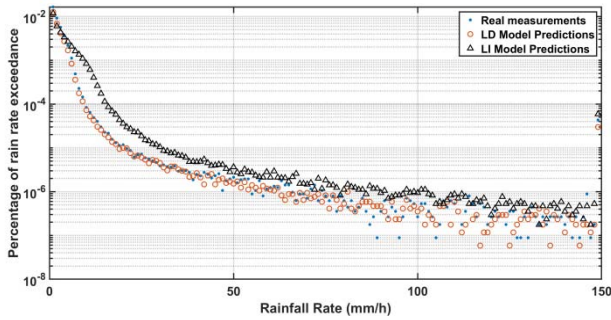
Fig. 9. CCDF of rainfall rate at Portsmouth for one month period.

Fig. 10. Test for log-Normality of rainfall rate distribution for the predicted rain field from the proposed models.

period, with the value of 8436 × 41 × 41, where 8436 is the number of 5 min rain maps available in the month and 41 × 41 is the number of points in the 205 × 205 km area. It has been demonstrated in [32] that the statistical distribution of rain will become stable and converge to constant values when the map size is greater than 200 × 200 km.

Taking the Portsmouth vicinity as an example, the complementary cumulative distribution function (CCDF) is plotted to test the exceeded rainfall rate using (10). The rain rate exceedance distributions estimates from the proposed models and radar measurements are presented in Fig. 9. The plot shows that the rainfall rate exceedance distributions estimates by the LD model are very close to the real measurements from radar data with relative root mean square (rms) error of 3.9371×10^{-4}. The rms error between distributions from the LI model estimates and measured data is slightly larger at 5.1709×10^{-4}. Taking $R_{0.001}$ as an example, the values from the LD model and radar data are 20 and 20.3 mm/h, respectively. However, $R_{0.001}$ from the LI model is 30.5 mm/h, almost 1.5 times the real measurements. This demonstrates that the LD model is more accurate than the LI model although both have small rms errors in general distribution. In addition, the probability of heavy rain events is extremely low, particularly for $R > 90$ mm/h, however large variation and the difference between model predictions and real measurements can be observed.

C. Rainfall Rate Distribution

It is widely accepted that the cumulative rain distribution exhibits log-Normality [3]. To test if the model predictions preserve the underlying properties of rain, the statistics of rainfall rate over the studied area using the histogram of rainfall rate conditioned on the actual occurrence of rain was calculated. Using the technique described in [40], the transformed CCDF can be achieved. If the data is log-normal, then the transformed CCDF shows up as a straight line.

Fig. 10 presents the test for the log-Normality of rainfall rate distribution. The straight lines demonstrate that the rainfall rate predicted by LI and LD models is log-normally distributed. It is salient to notice that the LD model gives almost the same result as the one from the radar estimates, implying that it is highly accurate. The calculated relative rms error is 0.0013. On the other hand, the accuracy of the LI model is quite
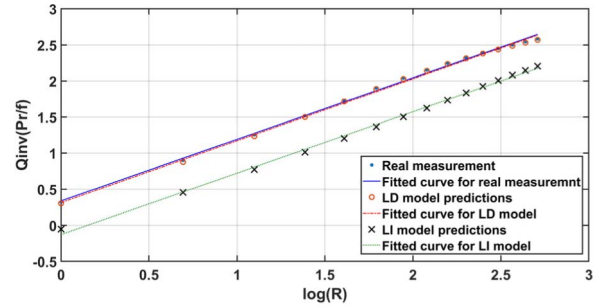
poor and there is a gap between the real measurements and model predictions. The calculated rms error is 0.473, almost 364 times of LD model.

VI. Discussion

Based on the description in Sections IV and V, we note that the accuracy of deep learning-based rain models is quite high. In particular, compared to the traditional rain models proposed in the last decades, i.e., the stochastic model [41], NWP model [42], and multifractal model [43], the deep learning-based rain model is more concise in form. In addition to that, the existing classical models always involve a lot of hand-crafted rain characteristics, complicated equations, and several preset assumptions for simplicity matter, such as the Taylor hypothesis in [44]. By contrast, the designed CNNs in deep learning-based models can determine and accurately grasp the underlying rain properties by themselves after learning a great deal of historical data.

However, the deep learning-based model also has its limitations, includes the following.

1) *Limited applicability:* Deep learning-based models are only applicable to the data available area and will be paralyzed for areas beyond the radar scan range, i.e., the gray areas in Fig. 1. This is because the network requires non-zero data with variations to train and learn, otherwise, it will lose its "prediction" ability.

2) *Low Flexibility:* The rainfall fields yielded by the deep learning-based models are not scaled continuously, but with a single (or multiple but discrete) and fixed space resolution in each training. If we need rain estimates at other space resolutions, readjustment of network parameters and retaining of input data will be required although the designed network could be unchanged. This certainly limits the models' flexibility and increases the computation load.

3) *Poor Accuracy at Super-High Resolution:* To further clarify the performance of the two proposed SRFICNNs, we adjusted the network parameters and studied the predictions at different spatial scales (for brevity, results are not presented in this article). Results show that our models can only improve the spatial resolution from 5 km to 500 m with reasonable accuracy. In other words, the maximum SF of the designed CNNs is 10. Beyond

that, the model will crash down as the accuracy is significantly reduced.

There might be two possible solutions for the above issues: 1) new CNNs design with better performance is required and 2) as the ability of the deep learning-based rain model is limited, external assistance might be needed to improve the model performance. The authors believe that an approach that combines better-performing CNNs with traditional numerical methods could be a potentially promising solution.

VII. CONCLUSION

This article has proposed two deep learning-based models (SRFICNNs) for predicting and simulating the rainfall fields across the U.K. at scales finer than are currently available from NIMROD rain radar. One of them is the LI model with its key task of determining the non-linear mapping relationship $\mathcal{F}(\cdot)$ between an LR rain rate and a higher one through studying a series of input data. The other is the LD model, which focuses on the study of the residual between the original and up-scaled rain maps.

The model predictions have been analyzed by looking into the MSE and SSIM. The small MSE and large SSIM are self-evident for the high accuracy and SSIM between model-predicted rainfall fields and radar-derived images. The particular strength of the deep learning-based model is that formulated rain characteristics, complicated mathematical equations, and preset assumptions can be avoided because the network can automatically exploit and explicitly grasp the underlying rain properties more accurately. This offers great convenience, although the potential physical principle hidden in the neural networks is not apparent.

From the experimental results, we have found that the LD model has a faster convergence speed and gives better performance than the LI model. We have also investigated how the network depth affects the models' performance. Results show that both MSE and SSIM are good insofar as we push the depth to 15–25 weight layers. However, further increases (particularly for layer No > 25) result in worse performance. Given that a large layer depth increases computational load significantly but achieves no additional contribution to network performance, the default depth value was set as 20 layers in the final networks as a trade-off between model accuracy and cost. The visual comparison shows that rainfall fields yielded by the LD model are very close to the radar-derived image in both rain intensity and horizontal rain field structure while the LI model tends to overestimate the point rainfall rate to a large extent. Quantitative analysis shows that the mean error function for LD and LI models are 0.0317 and 0.0852, respectively.

In addition, we have also validated these two models using another two important indexes, rain rate exceedance distribution and log-Normality property. The LD model gives very accurate estimates of these two important indexes with corresponding rms errors of 5.1709×10^{-4} and 0.0013, respectively. In comparison, overestimation can still be observed in the results from the LI model. So in general, modeling the residual is proven to be very pragmatic since the difference between ULR data and that of HR measured data is very small. The extremely high accuracy and fast convergence speed of the LD model are evidence of its high applicability in applications relating to satellite networks. It can be used in many applications, i.e., allocating additional satellite resources to sites with the worst conditions, site diversity techniques, and instantaneous joint fade experienced by all the links in an arbitrary microwave network. This is particularly true for satellite network systems where the optimization of an adaptive onboard common resource-sharing system and FMT requires detailed knowledge of the rain-induced attenuation statistics.

However, the proposed models are only valid for areas with available radar data and cannot produce rainfall rates with continuous spatial scales. Extra computation is required if data is required at other resolutions and this is the congenital problem of CNNs. In addition, the limitation of the proposed models is up-scaling to 500 m as further up-scaling causes poorer accuracy and this also reduces the models' applicability.

In conclusion, this article proposes a new approach that can be used to interpolate meteorological data into finer resolutions by taking advantage of deep learning techniques. This can be used to design an improved network to produce a better resolution rain rate with continuous resolution. This could be additionally exploited to predict rain rates at finer spatial and temporal scales simultaneously.

ACKNOWLEDGMENT

REFERENCES

[1] D. Sumbiri and T. J. O. Afullo, "An overview of rainfall fading prediction models for satellite links in Southern Africa," *Prog. Electromagn. Res. B*, vol. 90, pp. 187–205, 2021.

[2] A. D. Panagopoulos and J. D. Kanellopoulos, "On the rain attenuation dynamics: Spatial–temporal analysis of rainfall rate and fade duration statistics," *Int. J. Satell. Commun. Netw.*, vol. 21, no. 6, pp. 595–611, 2003.

[3] B. C. Gremont and M. Filip, "Spatio–temporal rain attenuation model for application to fade mitigation techniques," *IEEE Trans. Antennas Propag.*, vol. 52, no. 5, pp. 1245–1256, May 2004.

[4] K. S. Paulson and X. Zhang, "Simulation of rain fade on arbitrary microwave link networks by the downscaling and interpolation of rain radar data," *Radio Sci.*, vol. 44, no. 2, pp. 1–10, Apr. 2009.

[5] R. Nebuloni, C. Capsoni, M. Luccini, and L. Luini, "Assessment of rain fade mitigation techniques for high throughput satellites by a time series synthesizer," in *Proc. 9th Eur. Conf. Antennas Propag.*, Apr. 2015, pp. 13–17.

[6] R. F. Voss, "Random fractal forgeries," in *Fundamental Algorithms for Computer Graphics*. Berlin, Germany: Springer, 1985, pp. 805–835.

[7] B. Mandelbrot, "How long is the coast of Britain? Statistical self-similarity and fractional dimension," *Science*, vol. 156, no. 3775, pp. 636–638, 1967.

[8] S. Lovejoy and B. B. Mandelbrot, "Fractal properties of rain, and a fractal model," *Tellus A*, vol. 37A, no. 3, pp. 209–232, May 1985.

[9] R. Deidda, "Multifractal analysis and simulation of rainfall fields in space," *Phys. Chem. Earth, B, Hydrol., Oceans Atmos.*, vol. 24, nos. 1–2, pp. 73–78, Jan. 1999.

[10] H. Zhang, H. A. Loáiciga, D. Ha, and Q. Du, "Spatial and temporal downscaling of TRMM precipitation with novel algorithms," *J. Hydrometeorol.*, vol. 21, no. 6, pp. 1259–1278, Jun. 2020.

[11] E. Sharifi, B. Saghafian, and R. Steinacker, "Downscaling satellite precipitation estimates with multiple linear regression, artificial neural networks, and spline interpolation techniques," *J. Geophys. Res., Atmos.*, vol. 124, no. 2, pp. 789–805, Jan. 2019.

[12] G. Xu, X. Xu, M. Liu, A. Sun, and K. Wang, "Spatial downscaling of TRMM precipitation product using a combined multifractal and regression approach: Demonstration for South China," *Water*, vol. 7, no. 12, pp. 3083–3102, Jun. 2015.

[13] L. Luini and C. Capsoni, "The impact of space and time averaging on the spatial correlation of rainfall," *Radio Sci.*, vol. 47, no. 3, pp. 1–10, Jun. 2012.

[14] G. Yang, D. Ndzi, K. Paulson, M. Filip, and A.-H. Al-Hassani, "Rainfall rate field space-time interpolation technique for North West Europe," *Prog. Electromagn. Res. M*, vol. 83, pp. 93–107, 2019.

[15] A. O. Ayo, P. A. Owolawi, J. S. Ojo, and L. J. Mpoporo, "Rain impairment model for satellite communication link design in South Africa using neural network," in *Proc. 2nd Int. Multidisciplinary Inf. Technol. Eng. Conf. (IMITEC)*, Nov. 2020, pp. 1–8.

[16] N. Jiang, W. Chen, L. Lin, and T. Zhao, "Single image rain removal via multi-module deep grid network," *Comput. Vis. Image Understand.*, vol. 202, Jan. 2021, Art. no. 103106.

[17] R. Girshick, J. Donahue, T. Darrell, and J. Malik, "Region-based convolutional networks for accurate object detection and semantic segmentation," *IEEE Trans. Pattern Anal. Mach. Intell.*, vol. 38, no. 1, pp. 142–158, Jan. 2016.

[18] C. K. Snderby et al., "MetNet: A neural weather model for precipitation forecasting," 2020, *arXiv:2003.12140*.

[19] G. Yang, D. L. Ndzi, A.-H. Al-Hassani, M. Filip, and D. Paul, "Space-time modeling of rainfall rate for satellite networks," *IEEE Access*, vol. 8, pp. 70496–70504, 2020.

[20] K. S. Paulson, C. Ranatunga, and T. Bellerby, "A method to estimate trends in distributions of 1 min rain rates from numerical weather prediction data," *Radio Sci.*, vol. 50, no. 9, pp. 931–940, Sep. 2015.

[21] J. Polz, C. Chwala, M. Graf, and H. Kunstmann, "Rain event detection in commercial microwave link attenuation data using convolutional neural networks," *Atmos. Meas. Techn.*, vol. 13, no. 7, pp. 3835–3853, Jul. 2020.

[22] B. Kumar, R. Chattopadhyay, M. Singh, N. Chaudhari, K. Kodari, and A. Barve, "Deep learning–based downscaling of summer monsoon rainfall data over Indian region," *Theor. Appl. Climatol.*, vol. 143, nos. 3–4, pp. 1145–1156, Feb. 2021, doi: 10.1007/S00704-020-03489-6.

[23] C. Dong, C. C. Loy, K. He, and X. Tang, "Image super-resolution using deep convolutional networks," *IEEE Trans. Pattern Anal. Mach. Intell.*, vol. 38, no. 2, pp. 295–307, Feb. 2016.

[24] J. Kim, J. K. Lee, and K. M. Lee, "Accurate image super-resolution using very deep convolutional networks," in *Proc. IEEE Conf. Comput. Vis. Pattern Recognit. (CVPR)*, Jun. 2016, pp. 1646–1654.

[25] B. W. Golding, "Nimrod: A system for generating automated very short range forecasts," *Meteorolog. Appl.*, vol. 5, no. 1, pp. 1–16, 1998.

[26] K. S. Paulson, "Trends in the incidence of rain rates associated with outages on fixed links operating above 10 GHz in the Southern United Kingdom," *Radio Sci.*, vol. 45, no. 1, pp. 1–9, Feb. 2010, doi: 10.1029/2009RS004193.

[27] D. L. Harrison, S. J. Driscoll, and M. Kitchen, "Improving precipitation estimates from weather radar using quality control and correction techniques," *Meteorological Appl.*, vol. 7, no. 2, pp. 135–144, Jun. 2000.

[28] *Specific Attenuation Model for Rain for Use in Prediction Methods*, document 838-3, ITU-R, Geneva, Switzerland, 2005.

[29] R. K. Crane, *Electromagnetic Wave Propagation Through Rain*. Hoboken, NJ, USA: Wiley, 1996.

[30] T. L. Bell and P. K. Kundu, "Comparing satellite rainfall estimates with rain gauge data: Optimal strategies suggested by a spectral model," *J. Geophys. Res., Atmos.*, vol. 108, no. D3, pp. 1–15, Feb. 2003.

[31] M. Aharon, M. Elad, and A. Bruckstein, "K-SVD: An algorithmm for designing overcomplete dictionaries for sparse representation," *IEEE Trans. Signal Process.*, vol. 54, no. 11, pp. 4311–4322, Oct. 2006.

[32] G. Yang, D. L. Ndzi, B. C. Gremont, K. Paulson, M. Filip, and A.-H. Al-Hassani, "The impact of spatial–temporal averaging on the dynamic–statistical properties of rain fields," *IEEE Trans. Antennas Propag.*, vol. 67, no. 12, pp. 7505–7517, Dec. 2019.

[33] Y. Goodfellow, Y. Bengio, and A. Courville, *Deep Learning*. Cambridge, MA, USA: MIT Press, 2016.

[34] D. P. Kingma and J. Ba, "Adam: A method for stochastic optimization," in *Proc. Int. Conf. Learn. Represent.*, 2015, pp. 1–15.

[35] K. Simonyan and A. Zisserman, "Very deep convolutional networks for large-scale image recognition," in *Proc. Int. Conf. Learn. Represent.*, 2015, pp. 1–14.

[36] V. Nair and G. E. Hinton, "Rectified linear units improve restricted Boltzmann machines," in *Proc. 27th Int. Conf. Mach. Learn.*, 2010, pp. 807–814.

[37] Y. Lecun, L. Bottou, Y. Bengio, and P. Haffner, "Gradient-based learning applied to document recognition," *Proc. IEEE*, vol. 86, no. 11, pp. 2278–2324, Nov. 1998.

[38] Z. Wang, A. C. Bovik, H. R. Sheikh, and E. P. Simoncelli, "Image quality assessment: From error visibility to structural similarity," *IEEE Trans. Image Process.*, vol. 13, no. 4, pp. 600–612, Apr. 2004.

[39] *Characteristics of Precipitation for Propagation Modelling*, document 837-7, ITU-R, Geneva, Switzerland, 2017.

[40] M. Filip and E. Vilar, "Optimum utilization of the channel capacity of a satellite link in the presence of amplitude scintillations and rain attenuation," *IEEE Trans. Commun.*, vol. 38, no. 11, pp. 1958–1965, Nov. 1990.

[41] G. Yang, B. C. Gremont, L. Yang, M. E. Ibrahim, and L. Bai, "Space–time channel model for rain-affected communication networks," *IEEE Trans. Antennas Propag.*, vol. 67, no. 7, pp. 4768–4776, Jul. 2019.

[42] P. K. Kundu and T. L. Bell, "A stochastic model of space-time variability of mesoscale rainfall: Statistics of spatial averages," *Water Resour. Res.*, vol. 39, no. 12, pp. 1–15, Dec. 2003.

[43] D. Wolfensberger, A. Gires, I. Tchiguirinskaia, D. Schertzer, and A. Berne, "Multifractal evaluation of simulated precipitation intensities from the COSMO NWP model," *Atmos. Chem. Phys.*, vol. 17, no. 23, pp. 14253–14273, Dec. 2017.

[44] R. Deidda, "Rainfall downscaling in a space-time multifractal framework," *Water Resour. Res.*, vol. 36, no. 7, pp. 1779–1794, Jul. 2000.
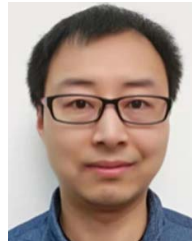
Guangguang Yang received the Diploma degree (Hons.) from the Xinxiang College, Xinxiang, China, in 2008, and the bachelor's degree (Hons.) and the Ph.D. degree in electronic engineering from the University of Portsmouth, Portsmouth, U.K., in 2010 and 2016, respectively.

He has been a Specially-Invited Researcher with the School of Electronic Information Engineering, Foshan University, Foshan, China, since 2019. He is currently the Deputy Secretary General of the organization of Foshan Electronics Association and a Juridical Person of Guangdong Daoli AI Technology Ltd., Guangzhou, China. His current research interests include Earth-space, terrestrial and wideband propagation, and applications relating to image processing and pattern recognition.

Zebin Chen is currently a Research Assistant with the School of Computer Science and Engineering, Sun Yat-sen University, Guangzhou, China. His current research interests include computer vision, computational photography, and machine learning.

David L. Ndzi received the B.Sc. degree (Hons.) in electronics and mathematics from Keele University, Newcastle, U.K., in 1994, and the Ph.D. degree in telecommunications from the University of Portsmouth, Portsmouth, U.K., in 1998.

He was the Faculty of Technology International Coordinator with the University of Portsmouth, until 2017. He is currently the Head of computing with the University of the West of Scotland, Paisley, U.K. His current research interests include wireless sensor networks and mesh networks for applications in environmental monitoring and prediction, behavioral economics, security, building control, and energy management.

Linda Yang received the B.E. and M.S. degrees in computer software and the Ph.D. degree in computer science from Peking University, Beijing, China, in 1993, 1996, and 1999, respectively.

She was a Lecturer with the Robert Gordon University, Aberdeen, U.K.; and a Senior Research Fellow with the University of St. Andrews and Cardiff University, Cardiff, U.K. She is currently a Senior Lecturer with the University of Portsmouth, Portsmouth, U.K. She was involved in U.K. and European funded research projects and published over 50 articles in refereed journals and conferences. Her current research interests include recommendation system, information retrieval, and data mining as well as their applications in social networks, health informatics, and business.

Dr. Yang is a member of the IET, WES, and HEA.

Abdul-Hadi Al-Hassani received the bachelor's degree from the University of Basra, Basrah, Iraq, in 1975, the master's degree from the University of Bradford, Bradford, U.K., in 1979, and the Ph.D. degree from Loughborough University, Loughborough, U.K., in 1983.

He is currently the General Director of the Basra Centre for Strategic Studies and also the Chancellor of the Iraq University College, Basrah. His current research interests include environmental monitoring and applications in construction and disaster prevention.

David C. Paul received the M.A. degree from the University of West London, London, U.K., in 1967.

He is currently a fellow of the Chartered Institute of Marketing, Manchester, U.K. His career in science, engineering, and technology business communications included consultancy and management roles with international science, technology, and medical publishers John Wiley, and divisions of Siemens, Groupe Schneider, Volvo, Fisons Scientific, and latterly, as the Director of corporate and business communications at the Global Engineering Group, ESAB. His specialization is in communicating complex topics in terms that are more accessible to senior decision-makers.

Zhikui Duan was born in Nei Mongolia, China, in 1985. He received the B.S. degree from Central South University, Changsha, China, in 2008, the M.S. degree from National University of Defense Technology, Changsha, in 2011, and the Ph.D. degree from Sun Yat-sen University, Guangzhou, China, in 2015.

Since 2016, he has been with Foshan University, Foshan, China. His current research interests include analog integrated circuits, radiation hardened by design, and chaos circuits.

Jun Chen received the M.S. degree in communication and information system from Shantou University, Shantou, China, in 2014, and the Ph.D. degree in information and communication engineering from Sun Yat-sen University, Guangzhou, China, in 2018.

His current research interests include computer vision, image processing, pattern recognition, multiple target tracking, and optical flow.